Acta Oceanol. Sin., 2019, Vol. 38, No. 1, P. 13–21
https://doi.org/10.1007/s13131-017-1132-x
http://www.hyxb.org.cn
E-mail: hyxbe@263.net

Seasonal characteristics and forcing mechanisms of the surface Kuroshio branch intrusion into the South China Sea

Jingsong Guo[1, 2], Zhixin Zhang[1, 2], Changshui Xia[1, 2*], Binghuo Guo[1, 2]

[1] Key Laboratory of Marine Science and Numerical Modeling, First Institute of Oceanography, Ministry of Natural Resources, Qingdao 266061, China

[2] Laboratory for Regional Oceanography and Numerical Modeling, Pilot National Laboratory of Marine Science and Technology (Qingdao), Qingdao 266061, China

Received 10 October 2017; accepted 2 November 2017

Abstract

Using observational data of Argos satellite-tracked drifters from 1988 to 2012, we analyzed seasonal characteristics of the surface Kuroshio branch (KB) intrusion into the South China Sea (SCS). The analysis results are as follows. The surface KB originates from the southern Balintang Channel (BLTC) and Babuyan Channel (BBYC). It begins in late September, reaches peak strength in November–December, and declines at the end of March. The mean speed of drifters along the KB path during their traverse of the Luzon Strait (LS) was 43% faster than during the two days before entering the LS for the flow originating from the southern BLTC, but there was a 24% increase in speed for the flow from the BBYC. The observations show that in winter, monthly-mean sea-level anomalies (SLAs) were positive southwest of Taiwan Island and extended to the northern LS. The SLAs were negative northwest of Luzon Island and extended to the southern LS, which acted like a pump, forcing a part of Kuroshio water westward into the SCS. The condition under which the KB forms was solved by a set of simplified motion equations. The results indicate that whether the KB can form depends upon the sea-level gradient at the central LS and region to the west, as well as the location, speed and direction of Kuroshio surface water when it enters the LS.

Key words: surface Kuroshio branch, Luzon Strait, forcing mechanisms

Citation: Guo Jingsong, Zhang Zhixin, Xia Changshui, Guo Binghuo. 2019. Seasonal characteristics and forcing mechanisms of the surface Kuroshio branch intrusion into the South China Sea. Acta Oceanologica Sinica, 38(1): 13–21, doi: 10.1007/s13131-017-1132-x

1 Introduction

The Luzon Strait (LS) is an opening between Taiwan Island and Luzon Island, and is the only passage connecting the South China Sea (SCS) to the Philippine Sea, which has complex bottom topography. The North Luzon Trench (NLT) is oriented south–north. The island chain of the LS and three major channels, the Bashi, Balintany and Babuyan, are on the eastern side of the NLT. On the west side of the NLT, there are two sections of the ridge in a north–south direction. The northern section is the Hengchun submarine ridge with depths shallower than 600 m, and the southern section of the ridge is deeper than 1 000 m (Fig. 1).

The Kuroshio traversing LS has three main current types shown in Fig. 1 (Hu et al., 2000; Caruso et al., 2006). The Kuroshio's main stream (KMS) moves northward through the LS and continues along the east coast of Taiwan Island, and the patterns of Kuroshio intruding into the SCS may be manifold, as classified in previous studies (e.g., Hu et al., 2000; Caruso et al., 2006; Nan et al., 2011). The two main types are referred to as the Kuroshio branch (KB) (Wyrtki, 1961; Guan, 1978), and the Kuroshio loop current (KLC) (Nitani, 1972; Yuan et al., 2006; Nan et al., 2011) and the anti-cyclonic eddy (Wang and Chern, 1987; Li et al., 1998). Since this anti-cyclonic eddy is a shed eddy (SE) from the KLC, Guo et al. (2013) combined the KLC and the shed eddy into one type, named it the KLC-SE type. In this study, we will focus on the KB type only.

Previous investigations found a warm and saline tongue-like feature extending westward from the LS to the south of the Taiwan Strait in winter, and regarded it as the evidence of the KB (Wyrtki, 1961; Nitani, 1972; Guan, 1978). In recent years, the existence of the KB was confirmed by new observations. For example, the Argos drifter observations showed clearly that there was a near-surface westward current between 20°–21°N in the northeastern SCS, entering the SCS through the LS (Centurioni and Niiler, 2004; Park and Oh, 2007; Hu et al., 2008). Both satellite images of the Advanced Very High Resolution Radiometer-Infrared Radiation (AVHRR-IR) (Ho et al., 2004) and maps of the absolute dynamic topography (Yuan et al., 2006) indicated that the KB flowed from northeast of the Luzon Island toward the area southwest of Taiwan Island. However, these studies described only the KB in the northwestern SCS. In order to investigate the formation of the KB, it is necessary to analyze the flows within the LS and east of the LS.

The potential forcing mechanisms associated with the Kuroshio intrusion have received substantial attention but are still under debate. The main viewpoints and debates are as follows. (1) Monsoon wind or wind stress curl acts as the main forcing

Foundation item: The National Key Research and Development Program of China under contract Nos 2016YFC1401403, 2016YFB0201103 and 2017YFA0604101; the Strategic Priority Research Program of Chinese Academy of Sciences under contract No. XDA11020301; the National Natural Science Foundation of China under contract No. 41206025; the China Ocean Mineral Resources R&D Association Program under contract No. DY135-E2-1-06.
*Corresponding author, E-mail: xiacs@fio.org.cn

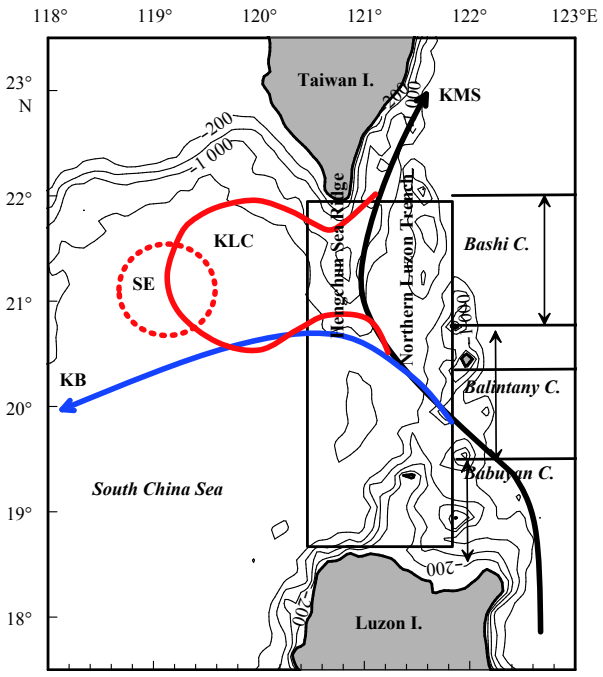

Fig. 1. Bathymetry of the Luzon Strait and the study region. The black, blue and red lines indicate the Kuroshio main stream (KMS), the Kuroshio branch (KB) and the Kuroshio loop current (KLC) and its shed eddy (SE), respectively.

mechanism of the Kuroshio intrusion (Shaw and Chao, 1994; Farris and Wimbush, 1996; Wang and Chern, 1987; Qu et al., 2000; Park and Oh, 2007). Centurioni et al. (2004, 2009), however, argued that the mean velocity of the westward current entering the SCS via the LS cannot be explained entirely in terms of the surface Ekman flow during the northeast monsoon. Using a multi-layer ocean general circulation model, Metzger and Hurlburt (2001) found that the Kuroshio intrusion was sensitive to instability and not related to the wind stress or its curl. Liang et al. (2008) also noted the monsoon-driven Ekman transport had little impact on the intrusion. (2) Sheremet (2001) suggested it was the balance between the beta effect carrying flow to the west and the inertia across the strait that governs the Kuroshio flowing across the LS. (3) Based on the analysis of satellite altimeter data, Zheng et al. (2011) suggested the essential mechanism of Kuroshio branching is the mesoscale eddy forcing or the interaction between the Kuroshio and mesoscale eddies originating from the subtropical Pacific. (4) Others concluded the seasonal variation of the Kuroshio transport or velocity at its upstream is the cause for the Kuroshio intrusion (Shaw et al., 1999; Yu et al., 2007; Sheu et al., 2010). Obviously, the mechanisms behind the Kuroshio intrusion are complicated and the forcing mechanisms of the KB and the KLC intrusion patterns might be different, so the debate continues.

In this paper, we focus on the KB entering the SCS via the LS, especially on what drives the intrusion. In Section 2, we describe the drifter data and delimit the study area. Sections 3 describes the statistical features of the KB. Section 4 presents physical and theoretical analyses on the forcing mechanisms of the KB. Conclusions and discussions are given in Section 5.

2 Data and methodology

The drifter data are from the Global Drifter Data Assembly Center at the Atlantic Oceanographic and Meteorological Laboratory (AOML) of NOAA. During the period from 1988 to 2012, there were more than 2 000 Argos drifters deployed in, or entering, the northwestern Pacific (5°–36°N, 122°–135°E), of which 147 Argos drifters passing through the LS. For the sake of clarity, these 147 drifter trajectories are shown in Fig. 2 in four periods. The position data of each drifter with 6-h interval are used to calculate mean speeds and draw their trajectories.

The LS includes the Bashi Channel (BSC), Balintany Channel (BLTC) and Babuyan Channel (BBYC). Its eastern boundary is the Luzon Island arc (Fig. 1), but its western boundary cannot be defined clearly. In order to calculate the duration and mean speed of each drifter passing through the LS, we delimit the rectangle region of 18.6°–22.0°N and 120.4°–121.9°E as the LS as in Guo et al. (2013); its western boundary is defined later using drifter trajectories. The three channels are regarded as the three entrances to the LS. The BSC is between Lanyu Island and Batan Island (22.0°–20.8°N). The BLTC is between Batan Island and Babuyan Island, of which (19.5°–20.2° N) is the southern BLTC and (20.2°–20.8° N) is the northern BLTC. The BBYC is between the Babuyan Island and the northeast coast of Luzon Island (19.5°–18.6°N) (Fig. 1).

3 Surface flow crossing the Luzon Strait

3.1 *Drifter path types and their occurrence probabilities*

We here separate the trajectories of the 147 drifters into three groups listed in Table 1, and then analyze their statistical characteristics.

The first group includes 62 drifter trajectories, which entered the LS across its eastern boundary, and then proceeded northward within the LS and entered the area east of Taiwan. This group indicates the path of the KMS type. One can see clearly from Table 1 and Fig. 2 that the KMS entered mainly from the southern BLTC and BBYC, and was confined to the region east of 120.4°E. This implies that the Kuroshio flows northward mainly along the North Luzon Trench. This result is consistent with previous hydrologic observations (Gilson and Roemmich, 2002) and numerical simulations (Metzger and Hurburt, 1996; Fang et al., 2003). The westernmost of the KMS trajectories reached 120.41°E in March, so longitude 120.4°E can be taken as the western boundary of both the surface Kuroshio and LS. The above results show only the statistical characteristics of part of the Kuroshio entering the LS. The other part flows northward just east of the LS and proceeds directly to the area east of Taiwan Island, without entering the LS.

The second group includes 71 drifters entering from various channels of the LS, which crossed the LS to enter the SCS and then retained a westward motion west of the LS. All these drifter trajectories occurred during the northeast monsoon (NEM) period, i.e., from the late September through March. The occurrence probability of the second group was 58% for 122 drifters entering the LS during the NEM period. We further subdivided these into three subgroups; their typical paths with the drifter trajectories are shown in Fig. 3. The first subgroup had 49 drifter trajectories, including 36 entering from the southern BLTC and 13 drifters from the BBYC that are indicated by "$C1_a$" in Tables 1 and 2. All 49 drifters entered the SCS passing though the west boundary of LS between the 20°–21°N. This subgroup of drifter trajectories effectively indicates the KB path from the traditional viewpoint shown in Fig. 1. The occurrence probability of drifters along the KB-type path was 69% for 71 second-group trajectories and 40% for 122 drifters entering the LS during the NEM period (late

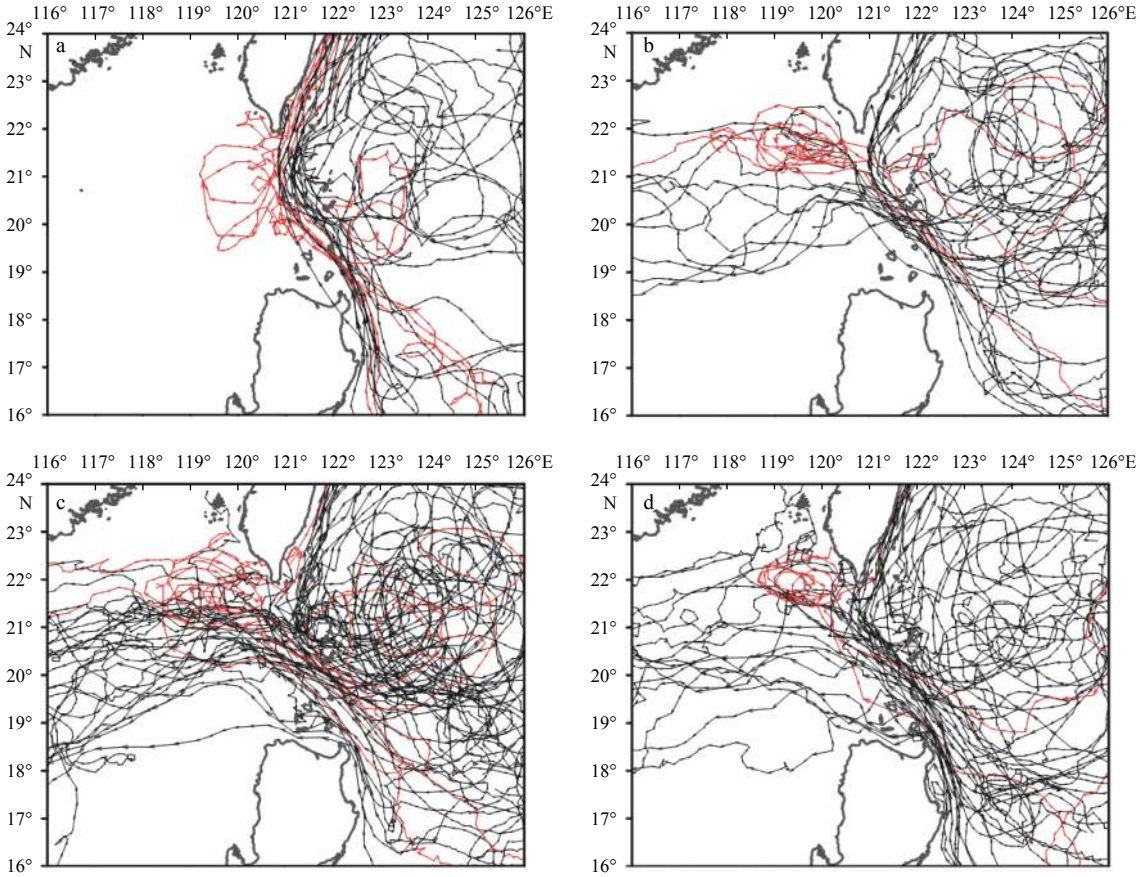

Fig. 2. Seasonal displacement diagrams of the drifters passed through the LS. a. April to mid-September; b. late September to October; c. November to December; and d. January to March. The red lines indicate the KLC-SE type of trajectory.

Table 1. Number of drifters for the three groups with trajectories through LS during the southwest monsoon period (SWMP i.e., April through mid-September) and northeast monsoon period (NEMP i.e., late September through March).

Tape	First group (KMS)					Second group					Third group (KLC-SE)			
	C1	C2	C3	C4	Tot.	$C1_{a/b}$	C2	C3	C4	Tot	C1	C2	C4	Tot
SWMP	4	15	1	1	21	0/0	0	0	0	0	4	0	0	4
NEMP	3	19	9	10	41	13/9	36	8	5	71	3	5	2	10
Tot	7	34	10	11	62	13/9	36	8	5	71	7	5	2	14

Note: C1, C2, C3 and C4 are Babuyan Channel (BBYC), southern Balintany Channel (BLTC), northern Balintany Channel (BLTC) and Bashi Channel (BSC), respectively. $C1_a$ and $C1_b$ indicate two subgroups of drifters entering LS from the BBYC, but $C1_a$ exited LS within 20°–21°N and $C1_b$ exited it south of 20°N, "Tot" is the sum.

September through March). The second subgroup had 13 trajectories entering from the northern BLTC and BSC. The third subgroup had 9 trajectories that entered from the BBYC, but entered the SCS passing though the west boundary of LS south of 20°N, which is indicated by "$C1_b$" in Tables 1 and 2. The second and third subgroups of drifter trajectories are different from the surface KB type in path and velocity obtained in following analysis.

The third group includes 14 trajectories (shown by the red lines in Fig. 2), in which seven drifters went along an anticyclonic loop path southwest of Taiwan Island and then returned to the Kuroshio (referred to as the KLC type), and six drifters moved along a small cyclonic path, as if following mesoscale eddies, after entering the area southwest of Taiwan Island (referred to as the shed eddy, or SE type). The two paths in the third type are named as the KLC-SE type, which were not investigated further.

3.2 *Speed changes along of the surface KB path*

To understand the character of the surface KB, we calculated the daily mean speed of each drifter and then the characteristic parameters. The latter included the duration and mean speed of each drifter passing through the LS, as well as the westward component of the mean speeds. The main statistical information of the first and second group drifters is listed in Tables 2 and 3. Figure 4 shows the mean speed difference ($\Delta\overline{V}$) of each drifter in the second group during the two days before and after they entered the LS. Figure 4 shows that the distribution of $\Delta\overline{V}$ samples was not uniform. Specifically, samples of the first subgroup drifters (KB type) were large and aggregated, but those of the second and third subgroup were fewer and scattered. Statistical information of the latter are also listed in Table 2 for reference.

Here, SO, ND, JFM and NM are late September to October, November to December, January to March and November to March, respectively. N is the number of drifter, $\overline{U}_B$ and $\overline{U}_A$ are the mean westward speeds in the two days before and after entering the LS, respectively. $\Delta\overline{U} = \overline{U}_A - \overline{U}_B$ are is the total average speed

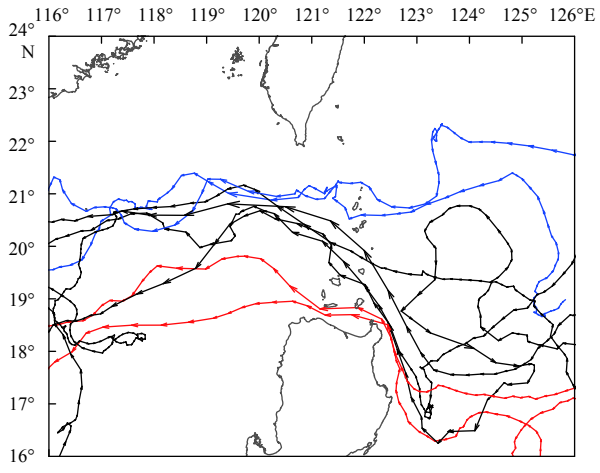

Fig. 3. Typical paths of the three subgroup drifters crossing the LS into the SCS. The black, blue and red lines indicate the first subgroup drifters ran along the KB path, the second subgroup drifters entered from the northern BLTC and the BSC, and the third subgroup drifters entered from the BBYC but ran out the LS south of 20°N, respectively.

increase. ($\Delta\overline{U}/\overline{U}_B$) is the total average speed increasing rate. *CI* is the confidence interval with level of 95%.

Average durations for crossing the LS to enter the SCS were 3.0–9.6 d for drifters entering from each channel, among which the minimum was that from the southern BLTC. This shows a pure inertia current of 28-h period is not a dynamic reason for Kuroshio water intruding into the SCS. For the KMS and KB characterized by drifter trajectories entering from the southern BLTC, their mean speeds of traverse through the LS were 53.0 and 81.9 cm/s, respectively, revealing that the former is obviously smaller than the latter.

$\overline{V}_c$ and $\overline{V}_B$ shown in Table 2 are total average speeds for the mean speed of each subgroup trajectories of second group drifters entering the LS during crossing the LS and two days before entering that strait. One sees from Table 2 that $\overline{V}_c$ values depend on the entrance (origin), i.e., the fastest was 81.9 cm/s for the southern BLTC, followed by 73.6 cm/s for the BBYC (i.e., Cl_a shown in Table 2). Comparing $\overline{V}_c$ and $\overline{V}_B$, we find some important differences. For drifters entering the LS from the southern BLTC, the total average speed increase $(\Delta\overline{V})$ reached 24.8 cm/s, with a mean increase rate of 43.4%. The region of speed increase with confidence level 95% was 17.8–34.8 cm/s. For drifters entering from the BBYC, among which 13 drifters of the Cl_a subgroup showed a mean speed increase of 14.4 cm/s, the mean increase rate was 24.3%, and the region of speed increase with confidence level 95% was 6.2–24.6 cm/s. Nine drifters of Cl_b subgroup had a mean speed decrease of –12.2 cm/s (Table 2). For drifters entering from the northern BLTC and BSC, half showed increasing speeds and half decreasing ones. Thus, the total average speed varied slightly, but this result is not sufficiently reliable statistically, owing to limited samples. The total average speed of KMS-type drifters from the southern BLTC increased slightly (5.3 cm/s), and that from the BBYC decreased significantly (Table 2). This shows the surface speed of the KMS entering the LS from the southern BLTC was not clearly influenced by the islands.

To further investigate the development and weakening process of the KB, Table 3 gives statistical results of the mean westward speed components $(\overline{U}_B$ and $\overline{U}_A)$ in the two days before and after entering the LS for the KB-type drifters from the southern BLTC in three periods. These were the late September through October, November–December and January–March. The results show that for the three periods, $\overline{U}_B$ values were very similar, about 43–45 cm/s, but $\overline{U}_A$ values all were larger than $\overline{U}_B$. Increases $(\overline{U}_A - \overline{U}_B)$ were 22.1, 31.0 and 24.2 cm/s, with increase rates of 49%, 69% and 57%, respectively.

The above facts show that the surface KB appears in late

Table 2. Durations and mean speeds of the first group (KMS-type) and three subgroups of second group drifters passing through LS, and mean speed of the drifters in the two days before entering the LS from different entrances in NEMP

Groups		EC	N	RT	$\overline{T}$	RV_C	$\overline{V}_C$	$\overline{V}_B$	$\Delta\overline{V}\pm\sigma$
First group (KMS-type)		C1	3	3.8–13.9	7.6	36.4–96.1	69.3	87.9	–18.6
		C2	19	3.9–9.1	6.1	28.4–80.3	53.0	47.7	5.3±16.2
		C3	9	3.7–12.5	7.1	19.2–79.8	40.3	38.8	1.5±19.4
		C4	10	2.9–10.2	5.5	22.4–60.5	37.6	28.7	8.9±14.2
Second group	(1) KB-type	$C1_a$	13	2.1–7.0	4.1	31.1–107.0	73.6	59.2	14.4±17.4
		C2	36	1.5–5.2	3.0	45.7–143.9	81.9	57.1	24.8±20.9
	(2)	C3	8	2.7–13.0	5.7	29.7–76.7	49.6	44.54	5.1±20.5
		C4	5	3.5–9.2	6.0	18.5–62.3	38.8	3.9	–5.0±17.3
	(3)	$C1_b$	9	2.0–12.0	4.0	36.7–117.9	74.1	86.3	–12.2±26.6

Note: $\overline{T} = \sum T/N, \overline{V}_C = \sum V_C/N, \overline{V}_B = \sum V_B/N, \Delta\overline{V} = (\overline{V}_C - \overline{V}_B)$. EC stands for entrance channel, N the number of drifters entering from an entrance. $\overline{T}$ the duration; $\overline{V}_C$ and $\overline{V}_B$ the total average values of the mean speed of each drifter passing through the LS and that during the two days before entering the LS, respectively; RT and RV_C respectively the range of $\overline{T}$ and $\overline{V}_C$; σ the standard deviation.

Table 3. Mean westward component speeds (cm/s) of the KB-type drifters in the two days before and after entering the LS from the southern BLTC and the BBYC

EC	Period	N	$\overline{U}_B$	$\overline{U}_A$	$\Delta\overline{U}\pm\sigma$	$\Delta\overline{U}/\overline{U}_B$	CI
C2	SO	9	44.8	66.9	22.1±14.3	0.49	16.7–27.5
	ND	17	44.7	75.7	31.0±18.4	0.69	23.8–48.2
	JFM	10	42.7	66.9	24.2±13.7	0.57	14.7–33.7
$C1_a$	Tot./N	36	44.1	71.3	27.2±18.9	0.62	20.7–33.7
	NM	13	44.9	59.6	14.7±16.4	0.33	5.4–24.1

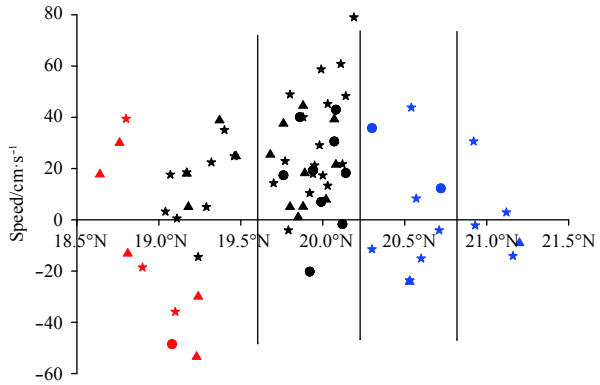

Fig. 4. Difference between the mean speed of the three subgroup drifters during crossing the LS and that in the two days before entering the LS. The dots, stars and triangles indicate the drifters during late September to October, November to December, and January to March, respectively. The black, blue and red lines indicate the first, second and third subgroup drifters, respectively.

September, reaches its peak strength in November–December and declines in late March, which is almost synchronous with the northeast monsoon over the northern SCS. We found that mean speeds of the surface KB passing through the LS were greater than those of the KMS, and the mean speed crossing the LS had a notable increase rate of 43.4% for entrance from the southern BLTC, and the increase rate of mean westward component reached 62%. For drifters entering from the BBYC, their mean speed increased by only 24.2%, and the mean westward component increased by 33%. It is clear that as the northward Kuroshio left the coastline of Luzon Island, its direction deflected westward; in particular, a part of the Kuroshio entered the LS form the BBYC because of its close proximity to the coastline.

4 Forcing mechanism of the KB intrusion into the SCS

4.1 *Physical analysis*

In this section, we investigate two questions: (1) why the seasonal mean speeds of drifters along the KB path increase when they cross the LS into the SCS, and (2) what are the forcing mechanisms of KB formation?

In the preceding section, we indicate that the pure inertia current cannot cross the LS, which is 165 km wide. The speed of the KMS changes slightly only, after it enters the LS from the southern BLTC, so the southern BLTC topography should not be a significant forcing mechanism of the KB intrusion into the SCS. In the following, we address the forcing of the NEM on the Ekman current and circulation around the LS.

Driving effects of monsoon wind on current include weather and season time scales. Average durations of the KB-type drifters crossing the LS to enter the SCS were 1.5–5.5 d (Table 2); with the addition of two days before entering the LS this became 3.5–7.2 d that correspond to a weather cycles. A gale transit duration is about one day, during which drifter locations may be east of or within the LS, or are not in these two areas. Thus, the drifter speed difference during the two days before entering the LS to crossing the LS may increase, decrease, or not change. Thus, the possibility of drifters entering the SCS increase, because it is located just inside of the LS on the gale transit date. Centurioni et al. (2009) estimated that a northeast monsoon of 10 m/s would produce a near-surface Ekman flow of 25 cm/s at most, much less than the speed of the near-surface current obtained from the satellite-tracked drifters. Based on these two reasons, the standard deviations (σ) of 14–21 cm/s in Tables 2 and 3 can be considered mainly products of the Ekman current. Therefore, in general, the Ekman currents have been removed for $\Delta\overline{V}$ and $\Delta\overline{U}$, but not for $\overline{V}_{\mathrm{C}}$, $\overline{V}_{\mathrm{B}}$, $\overline{U}_{\mathrm{C}}$ and $\overline{U}_{\mathrm{B}}$, because the Ekman current directions driven by the northeast winds are uniform across the local area. In addition, the above analysis shows that both the appearances of the KB-type drifters and NEM were nearly synchronous, so wind stress pulsating should be one of the driving forces of the surface KB.

The main role of the seasonal mean NEM is to establish the winter circulation mode. There is a cyclonic circulation along the SCS edge, and its formation is a time course. A western boundary current first occurs at the northwestern continental slope of SCS in the late September, develops progressively southward following the NEM to the southernmost SCS in November, and establishes the eastern boundary current to form a complete winter circulation mode in December (Zhang et al., 2016). This is consistent with the temporal evolution of KB development. However, what is the relationship between the KB and circulation in the northern SCS? Two observations were used to analyze this question.

Figure 5 shows temperature, salinity and potential density (σ_0) distributions along 121°E (Fig. 1), based on CTD data of 25 December 2003. We see that the 14–24°C isotherms and 23.5–25.5 isopycnics had distinct inclines toward the north between 20.5°N and 21.0°N. Geostrophic calculation results (with reference to 1 000 m depth) show a westward surface current with speed of 99 cm/s, and that the sea level dynamic height at 21.0°N was 28 cm higher than that at 20.5°N.

Using data from the archiving, validation and interpretation of satellite oceanographic data (AVISO), Fig. 6 shows mean sea-level anomalies (SLAs) for December of 2000–2010 in the LS and adjacent areas. This figure clearly shows the following. SLAs were negative northwest of the Luzon Island and extended eastward to the southern LS, but they were positive southwest of the Taiwan Island, extending eastward to the northern LS. Thus, there was a strong SLA gradient in the area 19.8°–21.3°N, 119.5°–121.3°E, which was accompanied by an increase of westward velocity. The latter two findings clearly show a close relationship between the KB and circulation in the northern SCS.

Regarding the sea-level rise southwest of the Taiwan Island and in the northern part of the LS in winter, we believe that the combined action of the northeast monsoon, topography and active mesoscale eddies is the basic dynamic cause. First, the western boundary current along the SCS western edge under NEM driving causes sea-level rise toward the coast. Second, the KLC and its shed eddies carrying Kuroshio water intrudes frequently southwest of the Taiwan Island (Li et al., 1998; Zheng et al., 2011; Guo et al., 2013). This results in a dominance of anticyclonic eddies with positive SLA in this area. Second, the area north of 20.5°N is northern part of the northeastern SCS. Its southwest part embraces the Dongsha Islands and Dongsha Sea submarine plateau, which blocks SEs moving southwestward along the shelf slope, causing them to stay for a short time southwest of the Taiwan Island. Third, the northern part of the area connects with the East China Sea through the Taiwan Strait. Southward wind stress driven by the NEM may offset the northward pressure gradient force formed by the sea-level tilt in the strait, which favors the accumulation of water southwest of the Taiwan Island. The accumulated water may extend to the northern LS. The geo-

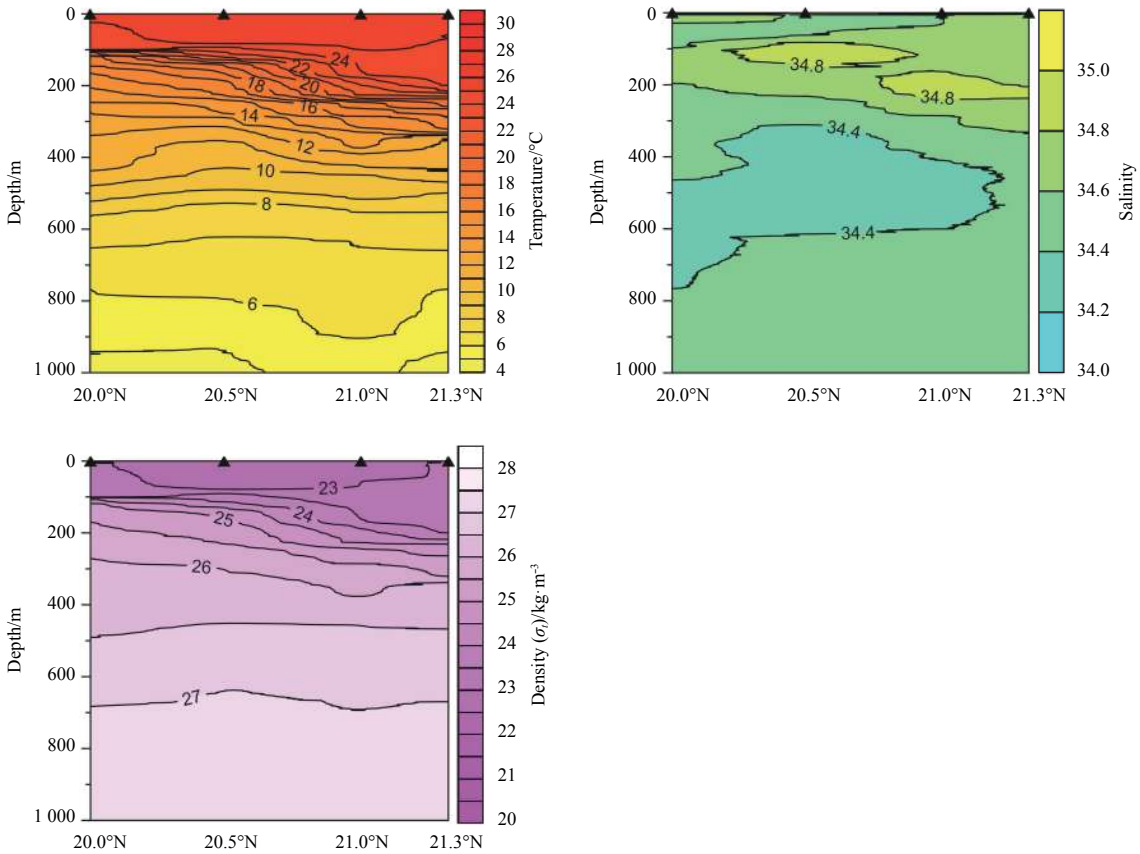

Fig. 5. Sections of temperature, salinity and density along 121°E on 25 December 2003.

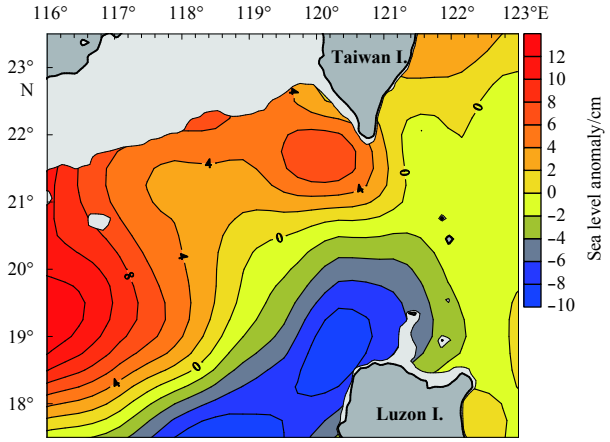

Fig. 6. Mean sea level anomaly (SLA) in the LS and its adjacent areas for the December of 2000–2010. The contour interval is 2 cm. The data are from the AVISO.

strophic current, which is related to the sea-level rise west of the LS, is part of the SCS circulation in winter.

The driving effects of the NEM on the circulation east of the LS mainly reflect the bifurcation latitude of the North Equatorial Current (NEC) northward shift during fall and winter (Sheu et al., 2010), which may slightly alter the Kuroshio current direction entering the LS.

The above analyses show that KB formation is directly related to the circulation and active mesoscale eddies west of the LS, and this relationship is not limited to the surface.

4.2 *Condition of the KB formation*

In order to inquire further the condition of the KB formation, a set of simplified equations with the consideration of both viscosity and the background current field (i.e., the Kuroshio) is used to describe the drifter movements tracking the KB. We here decompose the total velocity fields (U, V) into the background Kuroshio velocity (U_B, V_B) with geostrophic current property and their anomalies (u, v). The governing equations of the latter are given as follows:

$$\begin{aligned} \frac{\partial u}{\partial t} - fv + \mu u &= -g\frac{\partial \eta}{\partial x}, \\ \frac{\partial v}{\partial t} + fu + \mu v &= -g\frac{\partial \eta}{\partial y}, \end{aligned} \tag{1}$$

where f is the Coriolis parameter, and η is the SLA defined by removing the surface dynamic height of the background current, namely, the Kuroshio. The third term on the left hand side of the Eq. (1) is a simplified form of the viscosity term. μ is the viscous drag coefficient between the KB and the background filed.

The velocities entering the study area as shown in Fig. 1 are taken as the initial condition $(u, v)|_{t=0} = (u_0, v_0)$. The solution of the Eq. (1) is

$$\begin{aligned} u &= A\exp(-\mu t)\sin(ft+\alpha) + u_c, \\ v &= A\exp(-\mu t)\cos(ft+\alpha) + v_c, \end{aligned} \tag{2}$$

where $\alpha = \tan^{-1}[(u_0 - u_c)/(v_o - v_c], A = \left[(u_0 - u_c)^2 + (v_0 - v_c)^2\right]^{1/2}$, and

$$u_c = \frac{g}{f^2+\mu^2}\left[-\mu\frac{\partial\eta}{\partial x} - f\frac{\partial\eta}{\partial y}\right],$$
$$v_c = \frac{g}{f^2+\mu^2}\left[-\mu\frac{\partial\eta}{\partial y} + f\frac{\partial\eta}{\partial x}\right]. \quad (3)$$

Then, the total velocity fields (U, V) are given as

$$U = A\exp(-\mu t)\sin(ft+\alpha) + U_b + u_c,$$
$$V = A\exp(-\mu t)\cos(ft+\alpha) + V_b + v_c. \quad (4)$$

The first term on the right hand side of the Eq. (4) is the pure inertial current. The second and third terms are constant currents, which show that the inertial circular center moves with the velocity of (U_b+u_c) (eastward component) and (V_b+v_c) (northward component). The preceding analysis has shown that pure inertia current with 28 hour period is not a dynamic reason of Kuroshio water intruding into the SCS, so whether the surface current can cross the LS mainly depends on the constant current components $(U_b + u_c)$ and $(V_b + v_c)$.

For a better understanding of the velocity variability during drifters crossing the LS, we consider first an ideal case when $\partial\eta/\partial x = 0$, and obtain the constant current components of Eq. (4),

$$U_b + u_c = U_b - \frac{fg}{f^2+\mu^2}\frac{\partial\eta}{\partial y},$$
$$V_b + v_c = V_b - \frac{f\mu}{f^2+\mu^2}\frac{\partial\eta}{\partial y}. \quad (5)$$

In general, f is more than an order bigger than μ. As shown by the SLA data in Section 4.1, the sea surface rise in the northern LS formed a positive $\partial\eta/\partial y$ according to the Eq. (5). Comparing with the Kuroshio velocity (U_b and V_b), the westward-component of the surface flow velocity increases distinctly when the direction of the Kuroshio is northwestward, i.e., U_b<0, but the variation of the northward-component is not distinct. After the Kuroshio turns toward northeast near 21°N, U_b>0 and $\partial\eta/\partial y$→0; so, U→U_b. This shows that the flow entering the LS has to cross the background field of the Kuroshio before the Kuroshio turns toward northeast; otherwise, it would go north along with the Kuroshio. This shows that a sufficiently large u_c (i.e., with enough southward pressure gradient force) is the necessary condition for the KB form. The next step is to seek the critical value based on the Eq. (5).

For the mathematical expression of the velocity filed of the Kuroshio, it is convenient to adopt the Gaussian function approach in the X'OY' coordinate (Fig. 7), i. e.,

$$U_b' = 0,$$
$$V_b' = W\exp\left(-kx'^2\right), \quad (6)$$

where k is the attenuation coefficient. In the coordinate $X'OY'$, the Y'-axis directs northwestward along the Kuroshio central streamline (KCSL) with the maximum velocity and the azimuth (–θ) before turning northeastward near 21°N as shown in Fig. 7; the X'-axis is perpendicular to the Y'-axis and directs northeastward. We assume that the velocity of the Kuroshio is W along the central streamline and decreases to We^{-1} at the two boundaries, as shown in Fig. 7. Now, the Eq. (6) can be written as

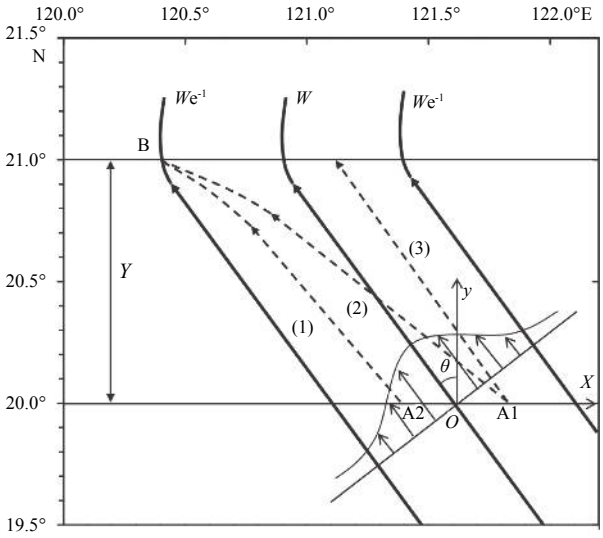

Fig. 7. Schematic diagram of the background current field of the Kuroshio and the drifter displacement paths. The thick lines denote the Kuroshio central streamline (KCSL) and boundaries with the velocities of W and We^{-1}, respectively. The thick arrows show the directions of the Kuroshio, and θ is the direction. The dotted lines denote the displacement paths of the drifters (1) beginning at A1 in the case without additional surface incline; (2) and (3) beginning at A1 and A2, respectively, and running out at B in the case with sea level incline anomaly.

$$U_b' + u_c' = u_c\cos\theta - v_c\sin\theta,$$
$$V_b' + v_c' = W\exp\left(-kx'^2\right) + u_c\sin\theta + v_c\cos\theta. \quad (7)$$

From Eq. (3), we can obtain

$$v_c = \lambda u_c, \quad (8a)$$

where

$$\lambda = \frac{\mu-\gamma f}{\gamma\mu+f}, \gamma = \frac{\partial\eta/\partial x}{\partial\eta/\partial y}, \quad (8b)$$

and γ is the direction of SLA slope. Substituting Eq. (8) into Eq. (7), integrating the resulted equations then yields the displacement of the particle

$$X' = \int_0^t (\cos\theta - \lambda\sin\theta)\, u_c dt = (\cos\theta - \lambda\sin\theta)\, u_c t, \quad (9)$$

$$Y' = \int_0^t W\exp\left(-kx'^2\right) dt + (\sin\theta + \lambda\cos\theta)\, u_c t. \quad (10)$$

From Eq. (9), we have

$$t = \frac{X'}{u_c(\cos\theta - \lambda\sin\theta)}. \quad (11)$$

For a small region where the drifters entered the SCS across the LS, γ is considered constant. Substituting Eq. (11) into Eq.

(10) gives

$$Y'_{\mathrm{B}}-Y'_{\mathrm{A}}=\left[\frac{\psi}{u_{\mathrm{c}}}+(\sin\theta+\lambda\cos\theta)(X'_{\mathrm{B}}-X'_{\mathrm{A}})\right](\cos\theta-\lambda\sin\theta)^{-1}, \quad (12)$$

where $\psi=\int_{X'_{\mathrm{A}}}^{X'_{\mathrm{B}}} W\exp\left(-kx'^{2}\right)\mathrm{d}x'$;

(X_{A}', Y_{A}') and (X_{B}', Y_{B}') are the positions of entering and leaving the calculation region (20°–21°N, 120.4°–121.9°E), respectively. Thus, the above equation can be rewritten as

$$\begin{aligned}u_{\mathrm{c}}=\psi/\left[(\cos\theta-\lambda\sin\theta)\left(Y'_{\mathrm{B}}-Y'_{\mathrm{A}}\right)\right.\\ \left.-(\sin\theta+\lambda\cos\theta)\left(X'_{\mathrm{B}}-X'_{\mathrm{A}}\right)\right],\end{aligned} \quad (13)$$

where

$$\begin{aligned}X'_{\mathrm{B}}-X'_{\mathrm{A}}&=(X_{\mathrm{B}}-X_{\mathrm{A}})\cos\theta-(Y_{B}-Y_{\mathrm{A}})\sin\theta,\\ Y'_{\mathrm{B}}-Y'_{\mathrm{A}}&=(X_{\mathrm{B}}-X_{\mathrm{A}})\sin\theta+(Y_{\mathrm{B}}-Y_{\mathrm{A}})\cos\theta.\end{aligned} \quad (14)$$

Now, we have obtained the relationship of the velocity u_{c} with the gradient direction of the SLA and the velocity and direction of the background Kuroshio. The preceding analysis indicates that the part of the Kuroshio fluid has to cross the LS before the Kuroshio turns to the northeastward direction, or else it follows the Kuroshio moving northward. Therefore, it is necessary to look for the minimum value of u_{c} (marked as u_{cs}), i.e., the minimum gradient of the SLA field, to ensure that a drifter can cross the LS. As an example of predicting u_{cs} using the Eq. (12), we assume that the position of (X_{A}', Y_{A}') entering the calculation region is at 20°N, in which A1 and A2 are on the east and west flanks of the Kuroshio, respectively. The position running out the LS (X_{B}', Y_{B}') is at 21°N, 120.4°E (Fig. 7). Other parameters are as follows:

$$\begin{aligned}&W=80\ \mathrm{cm/s},\ L=130\ \mathrm{km},\ \theta=30^{\circ},\\ &f=0.5\times10^{-4}\ \mathrm{s}^{-1},\ \mu=0.1\times10^{-4}\ \mathrm{s}^{-1},\\ &k=(2/L)^{-2}=2.37\times10^{-4}\mathrm{km}^{-2},\end{aligned}$$

where L is the width of the Kuroshio and k is the attenuation coefficient; then, we can calculate u_{cs} for different γ values. The calculation results are shown in Fig. 8. One can understand easily from Fig. 8 the possibility of flow crossing the LS. There is a great probability due to needing a small u_{cs} in the case that the SLA field has a northwestward gradient ($\gamma\leqslant0$), for example, the region of (20°–21.0°N, 119.5°–121.5°E) in Fig. 6 is such a region. When γ=–0.5 to 0.25, u_{cs} is about 20–45 cm/s for the current located at the central Kuroshio region. This result is consistent with the speed variation of drifters entering from the southern BLTC (Table 3). There is a small probability due to needing a great u_{cs} in the case of the SLA field with a northeastern slope (γ>0), and this probability is absent when γ>0.25, because a larger u_{cs} is required. We can use Fig. 8 to explain why the KB had a great increase in speed after entering the LS from the southern BLTC. Specifically, the drifters entering from the southern BLTC are located in the east-flank of the Kuroshio before reaching 20°N. So, a larger u_{cs} is required, and their speed increase is also great.

The above analysis results show the KB formation depends mainly on the gradient of SLA in the central LS and its west side, that are produced by the northern SCS circulation driven by the NEM and action of mesoscale eddies, as well as the position, velocity and direction of the background current when it enters the LS. The bifurcation latitude of the North Equatorial Current shifts northward and the Kuroshio transport deceases obviously in NEM period (Sheu et al., 2010); so, the Kuroshio entering the LS has a more westward direction and weaker velocity in the NEM period than that in the southwest monoon (SWM) period. The two reasons are conducive to the formation of the KB, and the second reason is consistent with the results in previous studies (Shaw et al., 1999; Yu et al., 2007; Sheu et al., 2010).

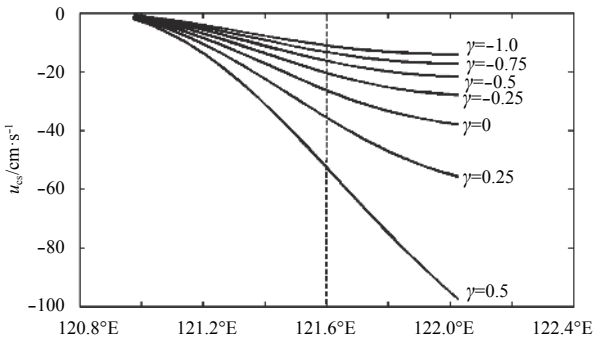

Fig. 8. Analytically-predicted values of u_{cs} to the longitude of drifter positions as entering calculation region for different SLA incline direction (γ), where γ varies from 0.5 to –1.0 with an interval of 0.25. The KCSL is at 121.6°E.

5 Summary and discussion

We analyzed the observational data of the Argos satellite-tracked drifters entering the LS from the North Pacific during 1988–2012, and described the statistical features of the surface KB. With both physical and theoretical analyses, we expounded the forcing mechanisms of the KB formation and reached the following conclusions.

The surface KB originates from the Kuroshio entering from the southern BLTC and BBYC, and separates from the Kuroshio between 20°–21°N near the western LS boundary. The surface KB appears in late September, reaches peak strength (in both speed and intrusion probability) during November–December, and declines in late March. Mean speeds of the surface KB traversing the LS are larger than those of the KMS. The mean speed of the surface KB crossing the LS has a notable increase rate of 43% for entrance from the southern BLTC. The mean speed of drifters entering from the BBYC increased by only 24%.

Physical analyses of the statistical results suggest the forcing effects of monsoon wind on the KB formation include weather and season time scales. For case of weather scales, the wind stress pulsating should be one of the driving forces of the surface KB. Main role of the seasonal mean NEM is to set up the winter circulation mode in the SCS, which is related to the seasonal variation of SLA west of the LS.

The oceanographic observations and the seasonal variation of SLA show that in winter, there was sea-level rise west of the LS that extended to the northern LS, and negative values (sea-level decline) northwest of Luzon Island extending to the southern LS. There was a northward SLA gradient and westward current between the two areas across 20°–21°N (Fig. 6). The circulation structure accompanying this winter dynamic topography west of the LS is similar to a pump, which forces a part of Kuroshio water westward into the SCS. We suggest this is the major forcing factor of KB formation, which is not limited to the surface.

The occurrence conditions of the KB were determined by a

set of simplified equations, with consideration of both viscosity drag and background current field. The results show that whether the KB can form depends mainly on the SLA gradient in the central LS and its west. In other words, there is a dependence on the circulation west of the LS and the entrance location, speed and direction of the Kuroshio when it enters the LS. These analyses also explain why the KB had a strong increase in speed after entering the LS.

References

Caruso M J, Gawarkiewicz G G, Beardsley R C. 2006. Interannual variability of the Kuroshio intrusion in the South China Sea. Journal of Oceanography, 62(4): 559–575, doi: 10.1007/s10872-006-0076-0

Centurioni L R, Niiler P P, Lee D K. 2004. Observations of inflow of Philippine Sea surface water into the South China Sea through the Luzon Strait. Journal of Physical Oceanography, 34(1): 113–121, doi: 10.1175/1520-0485(2004)034<0113:OOIOPS>2.0.CO;2

Centurioni L R, Niiler P N, Lee D K. 2009. Near-surface circulation in the South China Sea during the winter monsoon. Geophysical Research Letters, 36(6): L06605, doi: 10.1029/2008GL037076

Fang Guohong, Wei Zexun, Byung-Ho C, et al. 2003. Interbasin freshwater, heat and salt transport through the boundaries of the East and South China Seas from a variable-grid global ocean circulation model. Science in China Series D: Earth Sciences, 46(2): 149–161, doi: 10.1360/03yd9014

Farris A, Wimbush M. 1996. Wind-induced Kuroshio intrusion into the South China Sea. Journal of Oceanography, 52(6): 771–784, doi: 10.1007/BF02239465

Gilson J, Roemmich D. 2002. Mean and temporal variability in Kuroshio geostrophic transport south of Taiwan (1993–2001). Journal of Oceanography, 58(1): 183–195, doi: 10.1023/A:1015841120927

Guan Bingxian. 1978. The topographic effects of Taiwan Island, China and adjacent bottom relief on the path of the Kuroshio. Studia Marina Sinica (in Chinese), 14: 1–21

Guo Jingsong, Feng Yin, Yuan Yeli, et al. 2013. Kuroshio Loop Current intruding into the South China Sea and its shedding eddy. Oceanologia et Limnologia Sinica (in Chinese), 44(3): 537–544

Ho C R, Zheng Q, Kuo N J, et al. 2004. Observation of the Kuroshio intrusion region in the South China Sea from AVHRR data. International Journal of Remote Sensing, 25(21): 4583–4591, doi: 10.1080/0143116042000192376

Hu Jianyu, Kawamura H, Hong Huasheng, et al. 2000. A review on the currents in the South China Sea: seasonal circulation, South China Sea warm current and Kuroshio Intrusion. Journal of Oceanography, 56(6): 607–624, doi: 10.1023/A:1011117531252

Hu Xiaomin, Xiong Xuejun, Qiao Fangli, et al. 2008. Surface current field and seasonal variability in the Kuroshio and adjacent regions derived from satellite-tracked drifter data. Acta Oceanologica Sinica, 27(3): 11–29

Li Li, Nowlin W D Jr, Su Jilan. 1998. Anticyclonic rings from the Kuroshio in the South China Sea. Deep Sea Research Part I: Oceanographic Research Papers, 45(9): 1469–1482, doi: 10.1016/S0967-0637(98)00026-0

Liang W D, Yang Y J, Tang T Y, et al. 2008. Kuroshio in the Luzon strait. Journal of Geophysical Research, 113(C8): C08048, doi: 10.1029/2007JC004609

Metzger E J, Hurlburt H E. 1996. Coupled dynamics of the South China Sea, the Sulu Sea, and the Pacific Ocean. Journal of Geophysical Research, 101(C5): 12331–12352, doi: 10.1029/95JC03861

Metzger E J, Hurlburt H E. 2001. The nondeterministic nature of Kuroshio penetration and eddy shedding in the South China Sea. Journal of Physical Oceanography, 31(7): 1712–1732, doi: 10.1175/1520-0485(2001)031<1712:TNNOKP>2.0.CO;2

Nan Feng, Xue Huijie, Chai Fei, et al. 2011. Identification of different types of Kuroshio intrusion into the South China Sea. Ocean Dynamics, 61(9): 1291–1304, doi: 10.1007/s10236-011-0426-3

Nitani H. 1972. Beginning of the Kuroshio. In: Stommel H, Yoshida K, eds. Kuroshio: Its Physical Aspects. Tokyo: University of Tokyo Press, 129–163

Park G Y, Oh I S. 2007. Seasonal characteristics of the near-surface circulation in the northern South China Sea obtained from satellite-tracked drifters. Ocean Science Journal, 42(2): 89–102, doi: 10.1007/BF03020877

Qu Tangdong, Mitsudera H, Yamagata T. 2000. Intrusion of the North Pacific waters into the South China Sea. Journal of Geophysical Research, 105(C3): 6415–6424, doi: 10.1029/1999JC900323

Shaw P T, Chao S Y. 1994. Surface circulation in the South China Sea. Deep Sea Research Part I: Oceanographic Research Papers, 41(11–12): 1663–1683

Shaw P T, Chao S Y, Fu L L. 1999. Sea surface height variations in the South China Sea from satellite altimetry. Oceanologica Acta, 22(1): 1–17, doi: 10.1016/S0399-1784(99)80028-0

Sheremet V A. 2001. Hysteresis of a western boundary current leaping across a gap. Journal of Physical Oceanography, 31(5): 1247–1259, doi: 10.1175/1520-0485(2001)031<1247:HOAWBC>2.0.CO;2

Sheu W J, Wu C R, Oey L Y. 2010. Blocking and westward passage of eddies in the Luzon Strait. Deep Sea Research Part II: Topical Studies in Oceanography, 57(19–20): 1783–1791, doi: 10.1016/j.dsr2.2010.04.004

Wang J, Chern C S. 1987. The warm-core eddy in the northern South China Sea, I. Preliminary observations on the warm-core eddy. Acta Oceanographica Taiwanica, 18: 92–103

Wyrtki K. 1961. Physical oceanography of the Southeast Asian waters. Scientific results of marine investigations of the South China Sea and the Gulf of Thailand. NAGA Report, La Jolla, CA: Scripps Institution of Oceanography, 1–195

Yu Z, Shen S, McCreary J P, et al. 2007. South China Sea throughflow as evidenced by satellite images and numerical experiments. Geophysical Research Letters, 34(1): L01601, doi: 10.1029/2006GL028103

Yuan Dongliang, Han Weiqing, Hu Dunxin. 2006. Surface Kuroshio path in the Luzon Strait area derived from satellite remote sensing data. J Geophys Res, 111(C11): C11007, doi: 10.1029/2005JC003412

Zhang Zhixin, Guo Jingsong, Guo Binghuo. 2016. Reversal process of the South China Sea western boundary current in autumn 2011. Chinese Journal of Oceanology and Limnology, 34(3): 608–618, doi: 10.1007/s00343-016-4388-7

Zheng Quanan, Tai Changkuo, Hu Jianyu, et al. 2011. Satellite altimeter observations of nonlinear Rossby eddy–Kuroshio interaction at the Luzon Strait. Journal of Oceanography, 67(4): 365–376, doi: 10.1007/s10872-011-0035-2